



ELSEVIER

Available online at www.sciencedirect.com



Communications in
Nonlinear Science and
Numerical Simulation

Communications in Nonlinear Science and Numerical Simulation 12 (2007) 1534–1549

www.elsevier.com/locate/cnsns

Vibration analysis and bifurcations in the self-sustained electromechanical system with multiple functions

R. Yamapi ^{a,*}, M.A. Aziz-Alaoui ^b

^a *Department of Physics, Faculty of Sciences, University of Douala, P.O. Box 24157, Douala, Cameroon*

^b *Applied Mathematics Laboratory, University of Le Havre, 25 rue ph. Lebon, B.P 540, Le Havre, Cedex, France*

Received 11 February 2006; received in revised form 1 March 2006; accepted 1 March 2006

Available online 2 May 2006

Abstract

We consider in this paper the dynamics of the self-sustained electromechanical system with multiple functions, consisting of an electrical Rayleigh–Duffing oscillator, magnetically coupled with linear mechanical oscillators. The averaging and the harmonic balance method are used to find the amplitudes of the oscillatory states respectively in the autonomous and nonautonomous cases, and analyze the condition in which the quenching of self-sustained oscillations appears. The influence of system parameters as well as the number of linear mechanical oscillators on the bifurcations in the response of this electromechanical system is investigated. Various bifurcation structures, the stability chart and the variation of the Lyapunov exponent are obtained, using numerical simulations of the equations of motion.

© 2006 Published by Elsevier B.V.

PACS: 05.45.Xt; 85.85.+j

Keywords: Nonlinear dynamics; Self-sustained electromechanical in engineering systems

1. Introduction

The dynamics of self-excited coupled systems (including Van der Pol and Rayleigh equation) has received much attention over the last years [1–7]. This is due to the fact that such systems serve as a basic model of self-excited oscillation in physics, electronics, biology, neurology and many other disciplines.

Considering the forced coupled systems, our recent contributions are focussed to the dynamics of a nonlinear electromechanical system with multiple functions in series, consisting of the Duffing electrical oscillator magnetically coupled with linear mechanical oscillators [5,6]. The method of the harmonic balance has used to find the amplitude of the harmonic oscillatory states. The stability boundaries of the harmonic oscillations have also analyzed using the Floquet theory and the hysteresis effect. The effects of the number of linear mechanical oscillators on the behavior of the model have discussed and it appears that for some set of physical

* Corresponding author. Tel.: +237 932 93 76; fax: +237 340 75 69.

E-mail addresses: ryamapi@yahoo.fr (R. Yamapi), aziz.alaoui@univ-lehavre.fr (M.A. Aziz-Alaoui).

parameters, the undesired behaviors disappear with the increase of the number of the linear mechanical oscillators. Some bifurcation structures and the variation of the corresponding Lyapunov exponent have obtained. Transitions from a regular behavior to chaotic orbits are seen to occur for large amplitudes of the external excitation.

In the context of self-excited coupled systems, we studied recently the dynamics of the self-sustained electromechanical system (including the Rayleigh–Duffing equation) [7], consisting of an electrical Rayleigh–Duffing oscillator coupled magnetically and parametrically to a linear mechanical oscillator. Using the well-known analytical method, the behavior of the model has analyzed without discontinuous parameters before taking into account the effects of the discontinuous parameters. Various types of bifurcation structures were reported using numerical simulations of the equations of motion. An adaptive Lyapunov control strategy has enabled us to drive the system from the chaotic states to a targeting periodic orbit. In this paper, we extend our study by considering the dynamics of the self-sustained electromechanical system with multiple functions, but without discontinuous parameters, which consist of an electrical Rayleigh–Duffing oscillator coupled magnetically to n linear mechanical oscillators.

In this paper, we undertake an investigation of the dynamics of the self-sustained electromechanical system with multiple functions. We first analyze the behavior of the autonomous model before taking into account the effects of the external excitation. The paper is organized as follows. After presenting the physical model and giving the equations of motion in Section 2, we consider in Section 3 the behavior of the autonomous self-sustained model. The amplitudes of the oscillatory states and their stability are derived using the Averaging method [8,9], and we analyze its behavior when the parameters of the system vary. In Section 4, we consider the forced self-sustained electromechanical system and analyze the interaction of the external excitation with the amplitude of the limit cycle solution. We use the harmonic balance method [8,9] to derive the amplitudes of the harmonic oscillatory states and illustrate the effects of the number of mechanical oscillators. The phase difference between the linear mechanical oscillators is analyzed. We also analyze the bifurcation structures which appear in the model, and provide a stability chart, using numerical simulations based on the equations of motion. We note that all the numerical simulations are used the Runge–Kutta algorithm. The conclusion is given in Section 5.

2. Description and equations of motion

The model shown in Fig. 1 is the self-sustained electromechanical system with multiple functions, consisting of interacting electrical part (Rayleigh–Duffing oscillator) and mechanical part (linear oscillators). Both parts are coupled by the electromagnetic force developed by a permanent magnet. As a result, the Laplace force acts on the mechanical part, and the electromotive Lorenz force occurs in the electrical circuit. The electrical part of the system consists of a nonlinear resistor R , a nonlinear condenser C and an inductor L , all connected in series. One can consider the electromechanical model with the nonlinear electrical part obeying to the Rayleigh–Duffing equation. For this purpose, one makes use of two types of nonlinear components. The first type is the nonlinear capacitor with plate voltage V_c depending cubically on the charge q as

$$V_c = \frac{1}{C_0}q + a_3q^3, \tag{1}$$

where C_0 is the linear part of the capacitive characteristic and the parameter a_3 defines nonlinearity of the capacitor and depends on its type. This is typical of nonlinear reactance components such as varactor diodes widely used in many areas of electrical engineering to design, for instance, parametric amplifiers, up-converters, mixers, low-power microwave oscillators, etc. [10]. In the second type, the current voltage characteristic of a resistor [11] is also defined as

$$V_{R_0} = R_0i_0 \left\{ -\left\{ \frac{i}{i_0} \right\} + \left\{ \frac{i}{i_0} \right\}^3 \right\}, \tag{2}$$

where R_0 and i_0 are, respectively, the normalization resistance and current. i is the value of current corresponding to the limit resistor voltage. In this case, the model has the property to exhibit self-excited oscillations. This

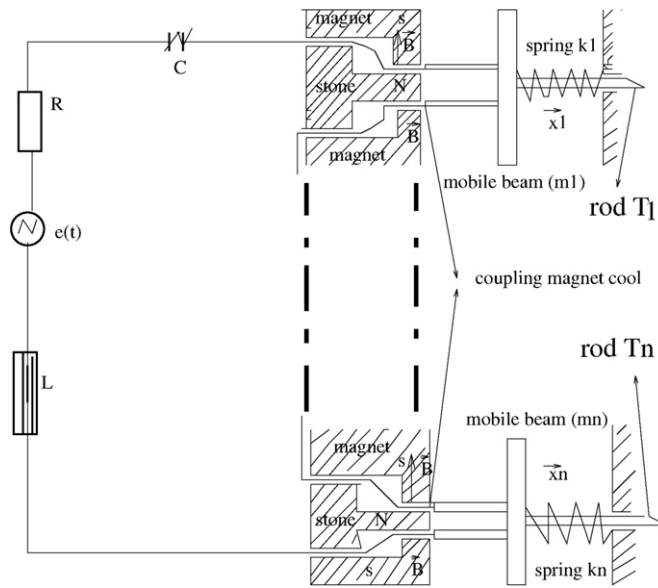


Fig. 1. Schema of the self-sustained electromechanical system with multiple functions.

is due to the presence of a nonlinear resistor where current–voltage characteristic curve shows a negative slope, and to the fact that the model incorporates through its nonlinear resistance a dissipative mechanism to damp oscillations that grow too large and a source of energy to pump up those that become small. Because of this particular behavior, we can qualify our model as a self-sustained electromechanical model. This nonlinear resistor can be realized using a block consisting of two transistors [12]. The mechanical part is composed of mobile beams which can move respectively along the \vec{z}_i ($i = 1, \dots, n$) axis on both sides. The rods T_i are bounded to mobile beams with springs of constants k_i . The electromechanical system with multiple functions obeys to the following $n + 1$ differential equations

$$\begin{aligned}
 L \frac{d^2 q}{d\tau^2} - R_0 \left\{ 1 - \frac{1}{i_0^2} \left(\frac{dq}{d\tau} \right)^2 \right\} \frac{dq}{d\tau} + \frac{q}{C_0} + a_3 q^3 + \sum_{i=1}^n l B_i \frac{dz}{d\tau} &= 0, \\
 m \frac{d^2 z_1}{d\tau^2} + \lambda^1 \frac{dz_1}{d\tau} + k_1 z_1 - l B_1 \frac{dq}{d\tau} &= 0, \\
 \vdots & \\
 m \frac{d^2 z_i}{d\tau^2} + \lambda^i \frac{dz_i}{d\tau} + k_i z_i - l B_i \frac{dq}{d\tau} &= 0, \\
 \vdots & \\
 m \frac{d^2 z_n}{d\tau^2} + \lambda^n \frac{dz_n}{d\tau} + k_n z_n - l B_n \frac{dq}{d\tau} &= 0,
 \end{aligned} \tag{3}$$

where L is an inductance in the electrical part, l is the length of the section of interaction of the magnetic field of intensity B_i with n moving rods to which a body of each mass m_i is attached, k_i is the coefficient of spring elastic stiffness, λ^i is the viscous friction coefficient, and \dot{q} is the current in the electrical circuit. Considering Q_0 as the reference charge of the condenser, and the following dimensionless variables

$$\begin{aligned}
 q = x Q_0, \quad z_i = l x_i, \quad t = w_e \tau, \quad w_e^2 = \frac{1}{LC_0}, \quad \beta = \frac{a_3 Q_0^3}{L w_e^2}, \quad w_{im}^2 = \frac{k_i}{m_i}, \quad w_i = \frac{w_m}{w_e}, \quad \mu = \frac{R_0}{L w_e}, \\
 \lambda_i = \frac{l^2 B_i}{L Q_0 w_e}, \quad \lambda_{i1} = \frac{B_i Q_0}{m_i w_e}, \quad \gamma_i = \frac{\lambda^i}{m_i w_e}, \quad \alpha_0 = \frac{Q_0^2 w_e^2}{i_0^2}
 \end{aligned}$$

the $n + 1$ differential equations yield to the following nondimensional equations:

$$\begin{aligned}
 \ddot{x} - \mu(1 - \alpha_0 \dot{x}^2)\dot{x} + x + \beta x^3 + \sum_{i=1}^n \lambda_i \dot{x}_i &= 0, \\
 \ddot{x}_1 + \gamma_1 \dot{x}_1 + w_1^2 x_1 - \lambda_{11} \dot{x} &= 0, \\
 \vdots & \\
 \ddot{x}_i + \gamma_i \dot{x}_i + w_i^2 x_i - \lambda_{i1} \dot{x} &= 0, \\
 \vdots & \\
 \ddot{x}_n + \gamma_n \dot{x}_n + w_n^2 x_n - \lambda_{n1} \dot{x} &= 0.
 \end{aligned} \tag{4}$$

where x and x_i are respectively, the dimensionless electric charge in the condenser and the displacement of each mobile beam. α_0 is the positive coefficient. For mathematical convenience, we set $\alpha_0 = 1$ in the rest of the paper. Thus, the equations of motion of the self-sustained electromechanical system with multiple functions consist of an electrical Rayleigh–Duffing oscillator coupled to linear mechanical oscillators.

The model shown in Fig. 1 is widely encountered in electromechanical engineering. In particular, in its linear version, it describes the well-known electrodynamic loudspeaker [13]. In this case, the sinusoidal signal $e(\tau)$ represents an incoming pure message. Because of the recent advances in the theory of nonlinear phenomena, it is interesting to consider such an electrodynamic system containing one or various nonlinear components or in the state where one or a number of its components react nonlinearly. One such state occurs in the electrodynamic loudspeaker due to the nonlinear character of the diaphragm suspension system resulting in signal distortion and subharmonic generation [13]. Moreover, the model can serve as a servo-command mechanism which can be used for various applications. Here one would like to take advantage of nonlinear responses of the model in manufacturing processes.

3. The resonant oscillatory states

3.1. The resonant oscillatory states and quenching phenomena

The amplitudes of the resonant oscillatory states of Eq. (4) can be found using the averaging method [8,9]. Following this method, we find that the amplitudes A and A_i of x and x_i , and the phase $\psi_i = \phi_i - \phi$ between x and x_i satisfy the following set of first-order differential equations:

$$\begin{aligned}
 \dot{A} &= -\frac{1}{2}\mu A \left(1 - \frac{3}{4}A^2\right) + \frac{1}{2} \sum_{i=1}^n \lambda_i w_i A_i \cos \psi_i, \\
 \dot{A}_1 &= -\frac{1}{2}\gamma_1 A_1 + \frac{\lambda_{11} A}{2w_1} \cos \psi_1, \\
 \vdots & \\
 \dot{A}_i &= -\frac{1}{2}\gamma_i A_i + \frac{\lambda_{i1} A}{2w_i} \cos \psi_i, \\
 \vdots & \\
 \dot{A}_n &= -\frac{1}{2}\gamma_n A_n + \frac{\lambda_{n1} A}{2w_n} \cos \psi_n, \\
 \dot{\psi}_1 &= -\frac{3}{8}\beta A^2 + \left\{ \frac{\lambda_{11} A}{2w_1 A_1} - \frac{\lambda_{11} w_1 A_1}{2A} \right\} \sin \psi_1, \\
 \vdots &
 \end{aligned}$$

$$\begin{aligned} \dot{\psi}_i &= -\frac{3}{8}\beta A^2 + \left\{ \frac{\lambda_{i1}A}{2w_iA_i} - \frac{\lambda_i w_i A_i}{2A} \right\} \sin \psi_i, \\ &\vdots \\ \dot{\psi}_n &= -\frac{3}{8}\beta A^2 + \left\{ \frac{\lambda_{n1}A}{2w_nA_n} - \frac{\lambda_n w_n A_n}{2A} \right\} \sin \psi_n. \end{aligned} \tag{5}$$

In the stationary state, the amplitudes A and A_i satisfy the following nonlinear equations:

$$\begin{aligned} \mu A_{as} \left(1 - \frac{3}{4}A_{as}^2 \right) &= \sum_{i=1}^n \lambda_i w_i A_{i(as)} \sqrt{1 - \frac{9\beta^2 w_i^2 A_{i(as)}^2 A_{as}^4}{16(\lambda_{i1}A_{as}^2 - \lambda_i w_i^2 A_{i(as)}^2)^2}}, \\ A_{i(as)}^2 &= M_i A_{as}^2 (4 - 3A_{as}^2), \\ M_i &= \frac{\mu \lambda_{i1}}{4n \gamma_1 \lambda_i w_i^2}. \end{aligned} \tag{6}$$

where A_{as} and $A_{i(as)}$ are the amplitudes of the stationary oscillatory state solutions. When the n linear mechanical oscillators are identical, Eq. (6) become

$$\begin{aligned} \frac{\mu^2 A_{as}^2 (1 - \frac{3}{4}A_{as}^2)}{n^2 \lambda_1^2 w_1^2 A_{1(as)}^2} + \frac{\frac{9}{16} \beta^2 w_1^2 A_{as}^6 A_{1(as)}^2}{(\lambda_{11}A_{as}^2 - \lambda_1 w_1^2 A_{1(as)}^2)^2} - 1 &= 0, \\ A_{i(as)}^2 &= M_i A_{as}^2 (4 - 3A_{as}^2). \end{aligned} \tag{7}$$

Eq. (7) can be solved using the Newton–Raphson algorithm or Mathematica code with the chosen set of parameters: $\lambda_{11} = 0.4$; $\lambda_1 := 0.08$; $\mu = 0.1$; $\beta = 0.5$; $w_1 = 1.0$. Fig. 2 shows the analytical and numerical response-curves when the damping coefficient γ_1 is varied. It appears a small disagreement between the results obtained from the analytical method and those obtained from the numerical method, this is due to the fact that the analytical results are derived through an averaging approximate method with need small value of μ . One finds that in the region of γ_1 defined as $\gamma_1 \in [0.251; 0.321]$, a complete quenching phenomena of oscillations occurs, In this state, the model can serve as an electromechanical vibration absorber [14] of undesirable self-excited vibrations in mechanical systems. The quenching of self-excited oscillations had also been reported in Refs. [11,15]. Here, the quenching of mechanical self-excited oscillations could be insured by an appropriate

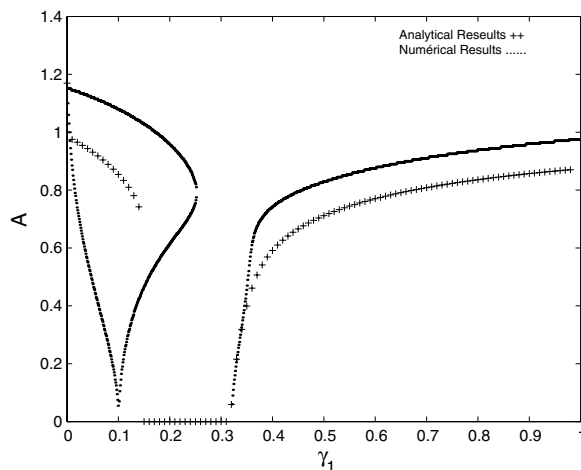


Fig. 2. Analytical and numerical limit cycle amplitude–response curves $A(\gamma_1)$. The parameters used are $\lambda_{11} = 0.4$; $\lambda_1 := 0.08$; $\mu = 0.1$; $\beta = 0.5$; $w_1 = 1.0$ and $n = 1$.

choice of the system parameters of an electrical circuit (assuming that the mechanical oscillator is described by the nonlinear oscillator and the electrical circuit by the linear oscillator). Analyzing the effects of the number n of the linear mechanical oscillators on the resonant oscillatory state solutions, we find that when the number n evolves, the resonant oscillatory state amplitude could not change. This is not surprising because the self-sustained electromechanical system has a similar behavior like that of a Van der Pol model, and therefore generates the limit cycle solution which does not depend on the number of linear mechanical oscillators and the system parameters. It is important to note that this limit cycle solution, is known to be a fairly strong attractor since it attracts all trajectories except the one initiated from the trivial fixed point.

3.2. Stability analysis

The stability of the resonant oscillatory state motions can be determined by investigating the nature of the stationary oscillatory state solutions of Eq. (5). To accomplish this, we let

$$\begin{aligned} A &= A_{as} + \delta A, \\ A_i &= A_{i(as)} + \delta A_i, \\ \psi_i &= \psi_{is} + \delta \psi_i, \end{aligned} \tag{8}$$

where ψ_{is} are the phases of the amplitudes of the stationary oscillatory state solutions. Substituting expressions (8) into Eq. (5), expanding for small δA , δA_i and $\delta \psi_i$ and keeping linear terms in δA , δA_i and $\delta \psi_i$, one obtains the following $2n + 1$ set of first-order differential equations

$$\begin{aligned} (\delta A)' &= -\frac{1}{2}\mu\left(1 - \frac{3}{4}A_{as}^2\right)\delta A + \frac{1}{2}\sum_{i=1}^n \lambda_i w_i (\delta A_i \cos \psi_i - \delta \psi_i A_{i(as)} \sin \psi_i), \\ (\delta A_1)' &= -\frac{1}{2}\gamma_1 \delta A_1 + \frac{\lambda_{11}}{2w_1} \{\delta A \cos \psi_1 - \delta \psi_1 A_{as} \sin \psi_1\}, \\ &\vdots \\ (\delta A_i)' &= -\frac{1}{2}\gamma_i \delta A_i + \frac{\lambda_{i1}}{2w_i} \{\delta A \cos \psi_i - \delta \psi_i A_{as} \sin \psi_i\}, \\ &\vdots \\ (\delta A_n)' &= -\frac{1}{2}\gamma_n \delta A_n + \frac{\lambda_{n1}}{2w_n} \{\delta A \cos \psi_n - \delta \psi_n A_{as} \sin \psi_n\}, \\ (\delta \psi_1)' &= \left\{ \frac{\lambda_{11}}{2w_1 A_{1(as)}} + \frac{\lambda_1 w_1 A_{1(as)}}{2A_{as}} \right\} \sin \psi_{1s} \delta A - \frac{3}{4} \beta A_{as} \delta A - \left\{ \frac{\lambda_{11} A_{as}}{2w_1 A_{1(as)}} + \frac{\lambda_1 w_1}{2A_{as}} \right\} \sin \psi_{1s} \delta A_1 \\ &\quad + \left\{ \frac{\lambda_{11} A_{as}}{2w_1 A_{1(as)}} - \frac{\lambda_1 w_1 A_{1(as)}}{2A_{as}} \right\} \cos \psi_{1s} \delta \psi_i, \\ &\vdots \\ (\delta \psi_i)' &= \left\{ \frac{\lambda_{i1}}{2w_i A_{i(as)}} + \frac{\lambda_i w_i A_{i(as)}}{2A_{as}} \right\} \sin \psi_{is} \delta A - \frac{3}{4} \beta A_{as} \delta A - \left\{ \frac{\lambda_{i1} A_{as}}{2w_i A_{i(as)}} + \frac{\lambda_i w_i}{2A_{as}} \right\} \sin \psi_{is} \delta A_i \\ &\quad + \left\{ \frac{\lambda_{i1} A_{as}}{2w_i A_{i(as)}} - \frac{\lambda_i w_i A_{i(as)}}{2A_{as}} \right\} \cos \psi_{is} \delta \psi_i, \\ &\vdots \\ (\delta \psi_n)' &= \left\{ \frac{\lambda_{n1}}{2w_n A_{n(as)}} + \frac{\lambda_n w_n A_{n(as)}}{2A_{as}} \right\} \sin \psi_{ns} \delta A - \frac{3}{4} \beta A_{as} \delta A - \left\{ \frac{\lambda_{n1} A_{as}}{2w_n A_{n(as)}} + \frac{\lambda_n w_n}{2A_{as}} \right\} \sin \psi_{ns} \delta A_n \\ &\quad + \left\{ \frac{\lambda_{n1} A_{as}}{2w_n A_{n(as)}} - \frac{\lambda_n w_n A_{n(as)}}{2A_{as}} \right\} \cos \psi_{ns} \delta \psi_n. \end{aligned} \tag{9}$$

The stability of the stationary oscillatory state solutions depends on the eigenvalues S of the coefficient matrix on the right-hand sides of Eq. (8). But due to the order of the Jacobian matrix $(2n + 1 \times 2n + 1)$, it is difficult to find the eigenvalue equation, we restrict our analysis to the case of one function ($n = 1$) and Eq. (9) become

$$\begin{aligned} (\delta A)' &= \Gamma_{11}\delta A + \Gamma_{12}\delta A_1 + \Gamma_{13}\delta\psi_1, \\ (\delta A_1)' &= \Gamma_{21}\delta A + \Gamma_{22}\delta A_1, \\ (\delta\psi_1)' &= \Gamma_{31}\delta A + \Gamma_{32}\delta A_1 + \Gamma_{33}\delta\psi_1, \end{aligned} \tag{10}$$

where the parameters Γ_{ij} are the elements of the Jacobian matrix (Γ) and are given by

$$\begin{aligned} \Gamma_{11} &= -\frac{1}{2}\mu\left(1 - \frac{9}{8}A_{as}^2\right), & \Gamma_{12} &= \frac{1}{2}\lambda_1 w_1 \cos\psi_{1s}, \\ \Gamma_{13} &= \frac{1}{2}\lambda_1 w_1 A_{as} \sin\psi_{1s}, & \Gamma_{21} &= \frac{\lambda_{11}}{2w_1} \cos\psi_{1s}, & \Gamma_{22} &= -\frac{1}{2}\gamma_1, \\ \Gamma_{31} &= -\frac{3}{4}\beta A_{as} + \left\{ \frac{\lambda_{11}}{2w_1 A_{1(as)}} + \frac{\lambda_1 w_1 A_{1(as)}}{2A_{as}} \right\} \sin\psi_{1s}, \\ \Gamma_{32} &= -\left\{ \frac{\lambda_{11} A_{as}}{2w_1 A_{1(as)}} + \frac{\lambda_1 w_1}{2A_{as}} \right\} \sin\psi_{1s}, \\ \Gamma_{33} &= \left\{ \frac{\lambda_{11} A_{as}}{2w_1 A_{1(as)}} - \frac{\lambda_1 w_1 A_{1(as)}}{2A_{as}} \right\} \cos\psi_{1s} \end{aligned}$$

Due to the Routh–Hurwitz, if the real parts of the roots of the characteristic equation of system (10) are negative, the corresponding stationary oscillatory state solutions is stable, if at least one root has a positive real part, the oscillatory state solution is unstable. The characteristic equation may be written as

$$S^3 + Q_1 S^2 + Q_2 S + Q_3 = 0, \tag{11}$$

where the coefficients Q_i are given as follows

$$\begin{aligned} Q_1 &= -\Gamma_{11} - \Gamma_{22} - \Gamma_{33}, \\ Q_2 &= \Gamma_{11}\Gamma_{22} + \Gamma_{33}(\Gamma_{11} + \Gamma_{22}) - \Gamma_{13}\Gamma_{31} - \Gamma_{23}\Gamma_{32} - \Gamma_{21}\Gamma_{12}, \\ Q_3 &= -\Gamma_{11}\Gamma_{22}\Gamma_{33} - \Gamma_{21}\Gamma_{32}\Gamma_{13} - \Gamma_{31}\Gamma_{12}\Gamma_{23} + \Gamma_{13}\Gamma_{31}\Gamma_{22} + \Gamma_{23}\Gamma_{31}\Gamma_{11} + \Gamma_{12}\Gamma_{21}\Gamma_{33}. \end{aligned}$$

The determination of signs of the real parts of the root S may be carried out by making use of the Routh–Hurwitz criterion [9]. In applying this criterion, we find that the real parts of the roots are negative if we have

$$\begin{aligned} Q_i &> 0 \quad (i = 1, 2, 3), \\ Q_1 Q_2 - Q_3 &> 0, \\ Q_3(Q_1 Q_2 - Q_3) &> 0, \end{aligned} \tag{12}$$

Additionally, the eigenvalues S of the Jacobian (Γ) are functions of the parameters of the system. Let us evaluate the trace $\text{tr}(\Gamma)$ and the determinant $\det(\Gamma)$ of A as

$$\begin{aligned} \text{tr}(\Gamma) &= Q_1, \\ \det(\Gamma) &= \Gamma_{11}\Gamma_{22}\Gamma_{33} - \Gamma_{21}\Gamma_{12}\Gamma_{33} + \Gamma_{21}\Gamma_{32}\Gamma_{13} - \Gamma_{31}\Gamma_{13}\Gamma_{22}, \end{aligned} \tag{13}$$

Considering the special case where at some parameters values $\mu = \mu_0$, one finds, through the Hopf theory, that the eigenvalue of the Jacobian matrix (Γ) is purely imaginary under the following transversally condition

$$\begin{aligned} \text{tr}(\Gamma) &= 0, \\ \det(\Gamma) &> 0. \end{aligned} \tag{14}$$

The two above conditions (12) and (14) are used to find the value of the μ_0 coefficient in which the eigenvalues S are purely imaginary and then define the curves (see Fig. 2) in which the amplitude oscillations (limit cycle) exists. Though the Hopf theory guarantees the existence of such periodic orbits for $\mu = \mu_0$, it does not guar-

antees the existence of the oscillations for the point μ furthest away from the point μ_0 . Often, however, the periodic orbit persists and grows in amplitude as $|\mu - \mu_0|$ increases.

4. The forced self-sustained electromechanical model

In this section, we find the interactions between the self-sustained oscillation and the external periodic forcing. One note that the frequencies of the forcing and the self-sustained oscillations are very important in the determination of the dynamics of the system. With the external force, the equations of motion become

$$\begin{aligned}
 \ddot{x} - \mu(1 - \dot{x}^2)\dot{x} + x + \beta x^3 + \sum_{i=1}^n \lambda_i \dot{x}_i &= E_0 \cos \omega t, \\
 \ddot{x}_1 + \gamma_1 \dot{x}_1 + \omega_1^2 x_1 - \lambda_{11} \dot{x} &= 0, \\
 \vdots & \\
 \ddot{x}_i + \gamma_i \dot{x}_i + \omega_i^2 x_i - \lambda_{i1} \dot{x} &= 0, \\
 \vdots & \\
 \ddot{x}_n + \gamma_n \dot{x}_n + \omega_n^2 x_n - \lambda_{n1} \dot{x} &= 0.
 \end{aligned} \tag{15}$$

where ω and E_0 are respectively the frequency and amplitude of the external excitation. Our aim is to study the interaction of the external excitation with the amplitude of the limit cycle solution and find various bifurcation structures which appear in the self-sustained electromechanical system.

4.1. The amplitude of harmonic oscillatory states

We derive in this subsection the amplitudes of the harmonic oscillatory states of the equations of motion (15). For this purpose, we suppose that the fundamental component of the solutions has a period of the sinusoidal voltage source. The harmonic balance method [8,9] enables us to find the solutions x and x_i in the form

$$\begin{aligned}
 x &= a_1 \cos \omega t + a_2 \sin \omega t, \\
 x_i &= b_{i1} \cos \omega t + b_{i2} \sin \omega t,
 \end{aligned} \tag{16}$$

Inserting Eq. (16) into Eq. (15) and equating the coefficients of $\sin \omega t$ and $\cos \omega t$ separately to zero (assuming that the terms due to higher frequencies can be neglected), we obtain

$$\begin{aligned}
 \left\{ 1 - \omega^2 + \frac{3}{4} \beta A^2 \right\} a_1 - \mu \omega \left\{ 1 - \frac{\omega^2}{4} A^2 \right\} a_2 + \sum_{i=1}^n \lambda_i \omega_i b_{i2} &= E_0, \\
 \mu \omega \left\{ 1 - \frac{\omega^2}{4} A^2 \right\} a_1 + \left\{ 1 - \omega^2 + \frac{3}{4} A^2 \right\} a_2 - \sum_{i=1}^n \lambda_i \omega_i b_{i1} &= 0, \\
 (\omega_1^2 - \omega^2) b_{11} + \gamma_1 \omega b_{12} - \lambda_{11} \omega a_2 &= 0, \\
 -\omega \gamma_1 b_{11} + (\omega_1^2 - \omega^2) b_{12} + \lambda_{11} \omega a_1 &= 0, \\
 \vdots & \\
 (\omega_i^2 - \omega^2) b_{i1} + \gamma_i \omega b_{i2} - \lambda_{i1} \omega a_2 &= 0, \\
 -\omega \gamma_i b_{i1} + (\omega_i^2 - \omega^2) b_{i2} + \lambda_{i1} \omega a_1 &= 0, \\
 \vdots & \\
 (\omega_n^2 - \omega^2) b_{n1} + \gamma_n \omega b_{n2} - \lambda_{n1} \omega a_2 &= 0, \\
 -\omega \gamma_n b_{n1} + (\omega_n^2 - \omega^2) b_{n2} + \lambda_{n1} \omega a_1 &= 0.
 \end{aligned} \tag{17}$$

It comes after some algebraic manipulations that the amplitudes of the harmonic oscillatory states satisfy the following nonlinear equations

$$\frac{9}{16}\beta^2 A^6 + \frac{3}{2}\beta F_n A^4 + (F_n^2 + G_n^2)A^2 - E_0^2 = 0, \tag{18}$$

$$A_i = \frac{\omega_i \lambda_{i1}}{\sqrt{D_i}} A,$$

where

$$A^2 = a_1^2 + a_2^2, \quad A_i^2 = b_{i1}^2 + b_{i2}^2,$$

$$D_i = (\omega_i^2 - \omega^2)^2 + \omega^2 \gamma_i^2,$$

$$F_n = 1 - \omega^2 - \sum_{i=1}^n \frac{\lambda_i \lambda_{i1} (\omega_i^2 - \omega^2)}{D_i},$$

$$G_n = -\mu\omega + \sum_{i=1}^n \frac{\lambda_i \lambda_{i1} \gamma_i \omega^3}{D_i},$$

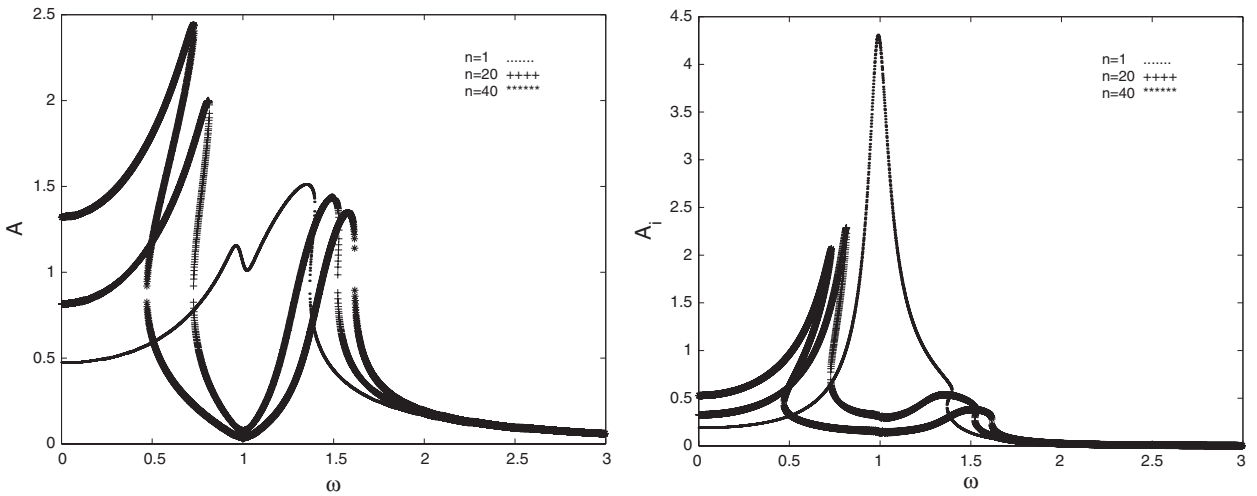


Fig. 3. Effects of the number of linear mechanical oscillators on the harmonic frequency–response curves $A(\omega)$ and $A_1(\omega)$ ($i = 1, \dots, n$). The parameters used are those of Fig. 2 and $E_0 = 0.5$, $\gamma_1 = 0.1$.

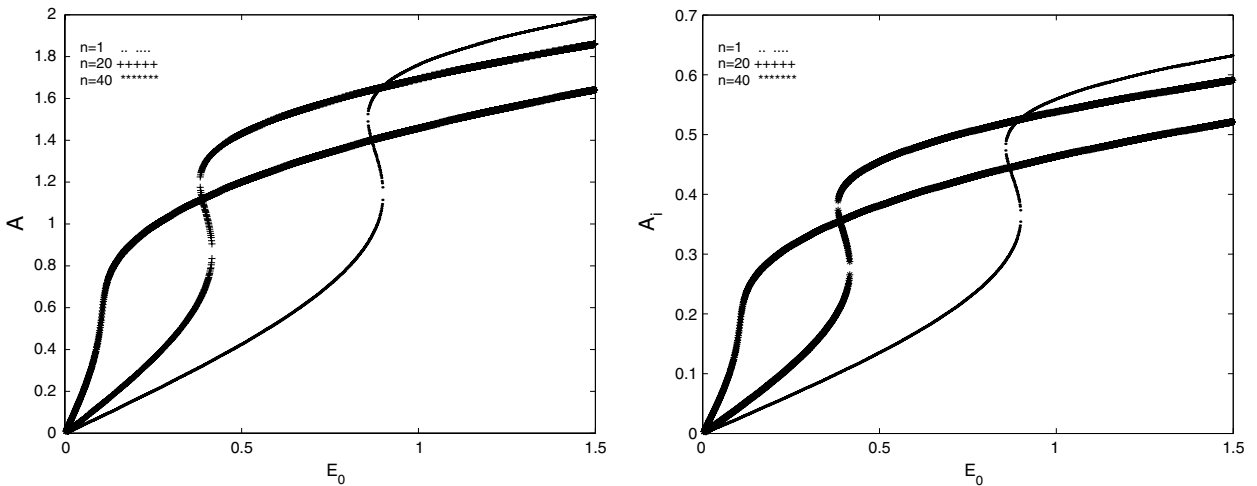


Fig. 4. Effects of the number of linear mechanical oscillators on the harmonic amplitude–response curves $A(E_0)$ and $A_1(E_0)$ ($i = 1, \dots, n$). The parameters used are those in Fig. 3 and $\omega = 1.5$.

In the presence of the external excitation, we provide in Fig. 3 the frequency–response curves for several different values of the number of the linear mechanical oscillators. It appears that the curves show antiresonance and resonance peaks, and the hysteresis phenomenon for some values of n . It is important to note that around the resonance peaks, the amplitudes and the accumulate energies of the self-sustained electromechanical device are higher than those received in any oscillations. In this case, the self-sustained model can give more interesting applications in electromechanical engineering, particularly when the model is used as a perforator electromechanical device, but the model with high energies is very dangerous since it can give rise to catastrophe damage. In the antiresonance peaks, the self-sustained electromechanical device vibrates with small amplitude and accumulates energy. This phenomena is of particular interest when the model is used as an electromechanical vibration absorber [10]. In Fig. 3, the effects of a number of linear mechanical oscillators are observed and the curves also show the resonance and antiresonance peaks, and hysteresis phenomena when the number n increases. We note that the multiplicity of the response curves due to cubic nonlinearity has a significant impact from the physical point of view because it leads to jump and hysteresis

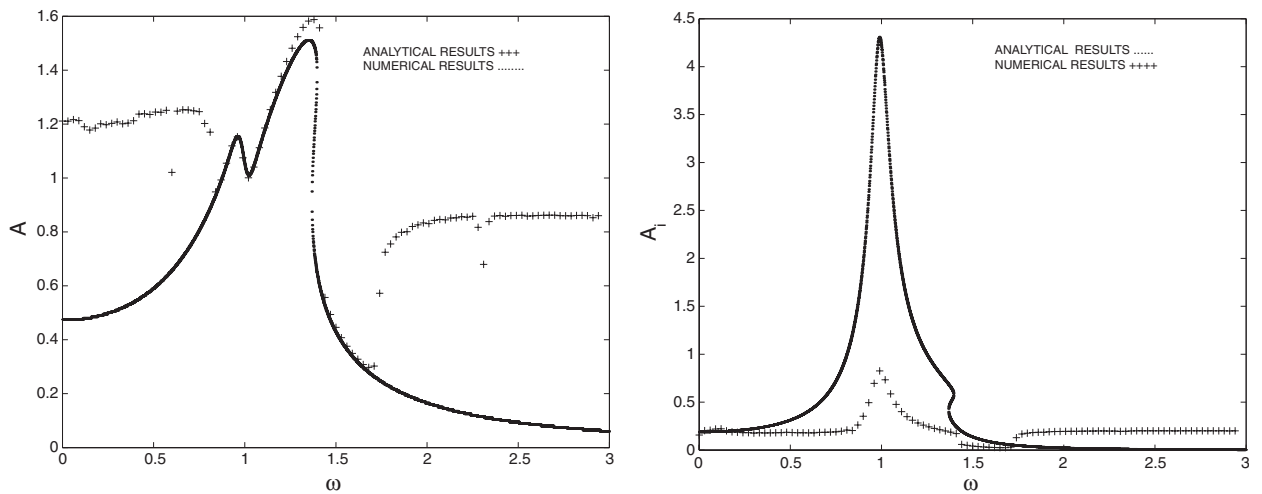


Fig. 5. Comparison between analytical and numerical results. The parameters used are those of Fig. 3 and $n = 1$.

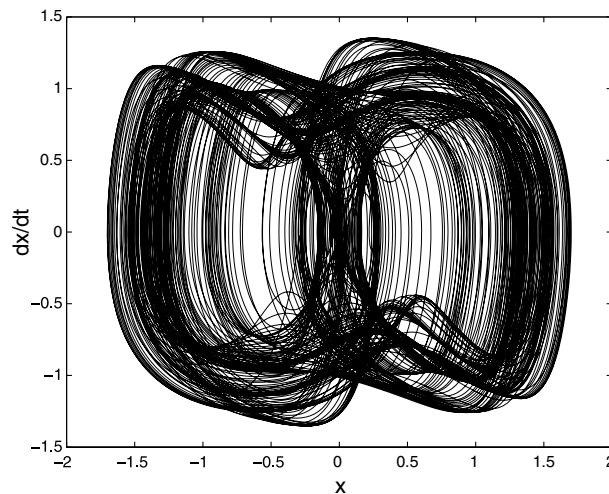


Fig. 6. Chaotic phase portrait of the forced self-sustained electromechanical system with the parameters $\mu = 2$; $\gamma_1 = 0.1$; $\lambda_1 = 0.4$; $\lambda_{11} = 0.2$; $w_1 = 1.0$; $\beta = 0.8$; $w = 1.0$; $n = 25$ and $E_0 = 13.0$.

phenomena with two stable amplitudes. Consequently, the self-sustained electromechanical device can vibrate in these domains with two different amplitudes of the harmonic oscillations depending on the initial conditions. Fig. 4 provides the amplitudes–response curves $A(E_0)$ and $A_f(E_0)$ for several values of n . This figure illustrates the effects of the number n of the linear mechanical oscillators on the behavior of the self-sustained electromechanical system. The following findings are observed. In the case of the model with one function, $A(E_0)$ and $A_f(E_0)$ show the jump phenomena, which disappear for the increasing of the number n of linear mechanical oscillators. For instance, with the parameters of Figs. 3 and 4, the disappearance of the jump phenomenon is obtained when the number n increases, in this case it is interesting to see that a further increase of the number n can absorb the jump phenomenon. Fig. 5 shows the comparison between analytical and numerical frequency–response curves. The discrepancy of the results obtained from the analytical method as compared to that obtained from the numerical method is observed for some region of w . This is due to the fact that one assume that the fundamental component of the solutions has a period of the sinusoidal voltage source, in which ignore the solution in the autonomous system.

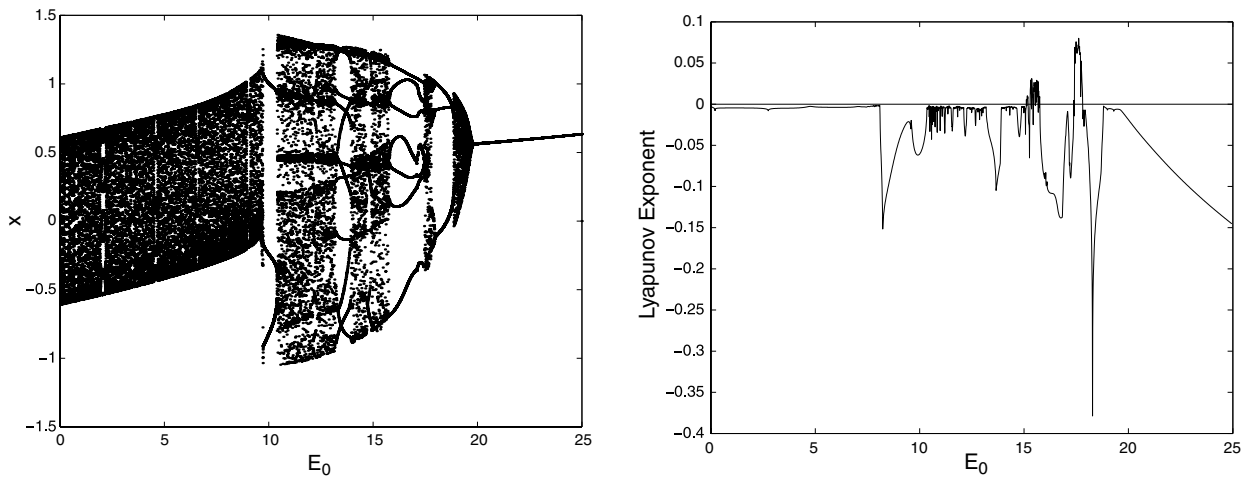


Fig. 7. Bifurcation diagram and Lyapunov exponent versus the amplitude E_0 with the parameters of Fig. 6.

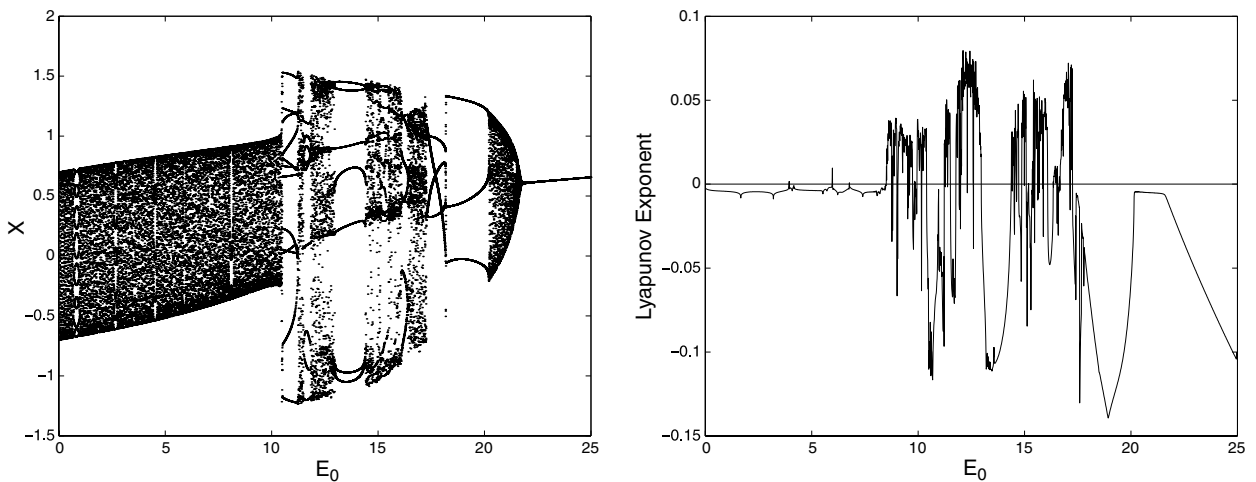


Fig. 8. Bifurcation diagram and Lyapunov exponent versus the amplitude E_0 with the parameters of Fig. 6 and $\mu = 4$.

4.2. Phase difference between the mechanical oscillators

In practical engineering use, it is important to analyze the phase difference between the linear mechanical oscillators. To this aim, we find through Eqs. (16) and (17) that the phases ϕ_i and ϕ_{i+1} of the i th and $(i + 1)$ th linear mechanical oscillators are given by

$$\tan \phi_i = \frac{b_{i2}}{b_{i1}} = \frac{(w_i^2 - w^2)(F_i + \frac{3}{4}\beta A^2) + \gamma_i w^2(G_i + \frac{1}{4}\mu w^3 A^2)}{(w_i^2 - w^2)(G_i + \frac{1}{4}\mu w^3 A^2) - w\gamma_i(F_i + \frac{3}{4}\beta A^2)},$$

$$\tan \phi_{i+1} = \frac{b_{(i+1)2}}{b_{(i+1)1}} = \frac{(w_{i+1}^2 - w^2)(F_{i+1} + \frac{3}{4}\beta A^2) + \gamma_{i+1} w^2(G_{i+1} + \frac{1}{4}\mu w^3 A^2)}{(w_{i+1}^2 - w^2)(G_{i+1} + \frac{1}{4}\mu w^3 A^2) - w\gamma_{i+1}(F_{i+1} + \frac{3}{4}\beta A^2)}.$$
(19)

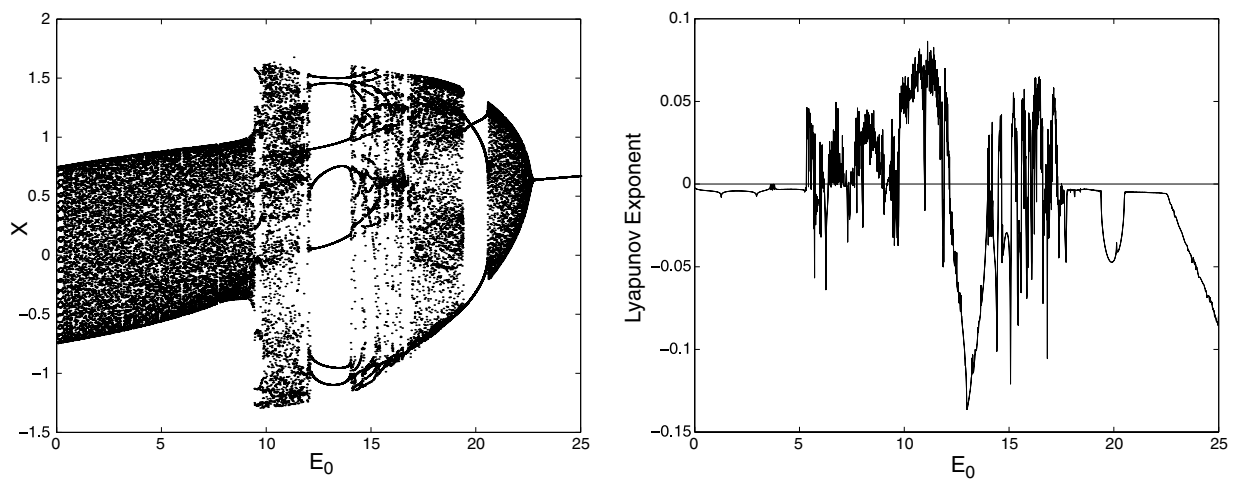


Fig. 9. Bifurcation diagram and Lyapunov exponent versus the amplitude E_0 with the parameters of Fig. 6 and $\mu = 5$.

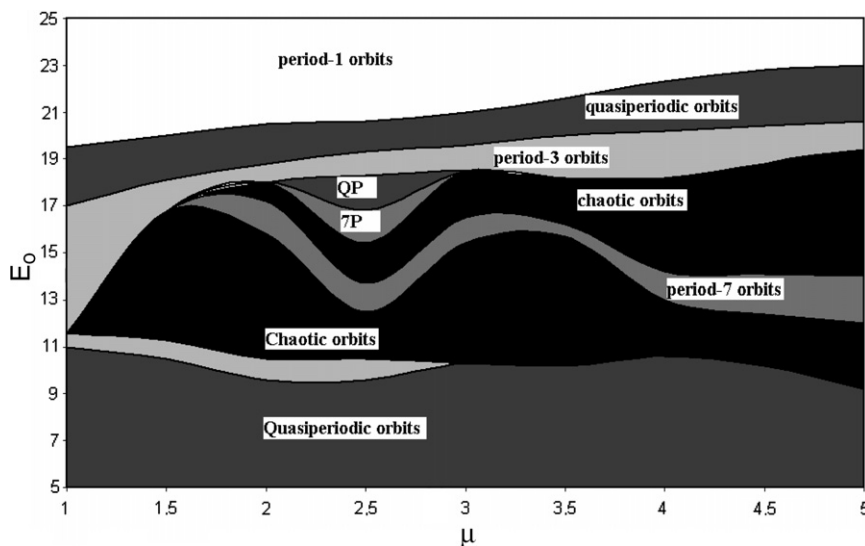


Fig. 10. Stability chart in the (E_0, μ) plane with the parameters of Fig. 6.

The phase difference is then defined as

$$\Theta_{i,i+1} = \frac{\phi_i - \phi_{i+1}}{w} \tag{20}$$

Our aim is to find the conditions in which all the linear mechanical oscillators vibrate in phase (phase-locked). One finds that all the linear mechanical oscillators are phase-locked in the following two situations:

- When all the $n + 1$ oscillators (electrical and n linear mechanical oscillator) enter in resonance (internal resonance $w_i = 1$) and for a fixed frequency w , $\Theta_{i,i+1}$ remains constant as the others parameters of the system vary.
- When all the $n + 1$ oscillators enter in internal ($w_i = 1$) and external ($w_e = 1$) resonance, all the i th and $(i + 1)$ th linear mechanical oscillator vibrate in phase and we have

$$\tan \phi_i = \tan \phi_{i+1} = \frac{w(G_i + \frac{1}{4}\mu w^3 A^2)}{F_i + \frac{3}{4}\beta A^2}. \tag{21}$$

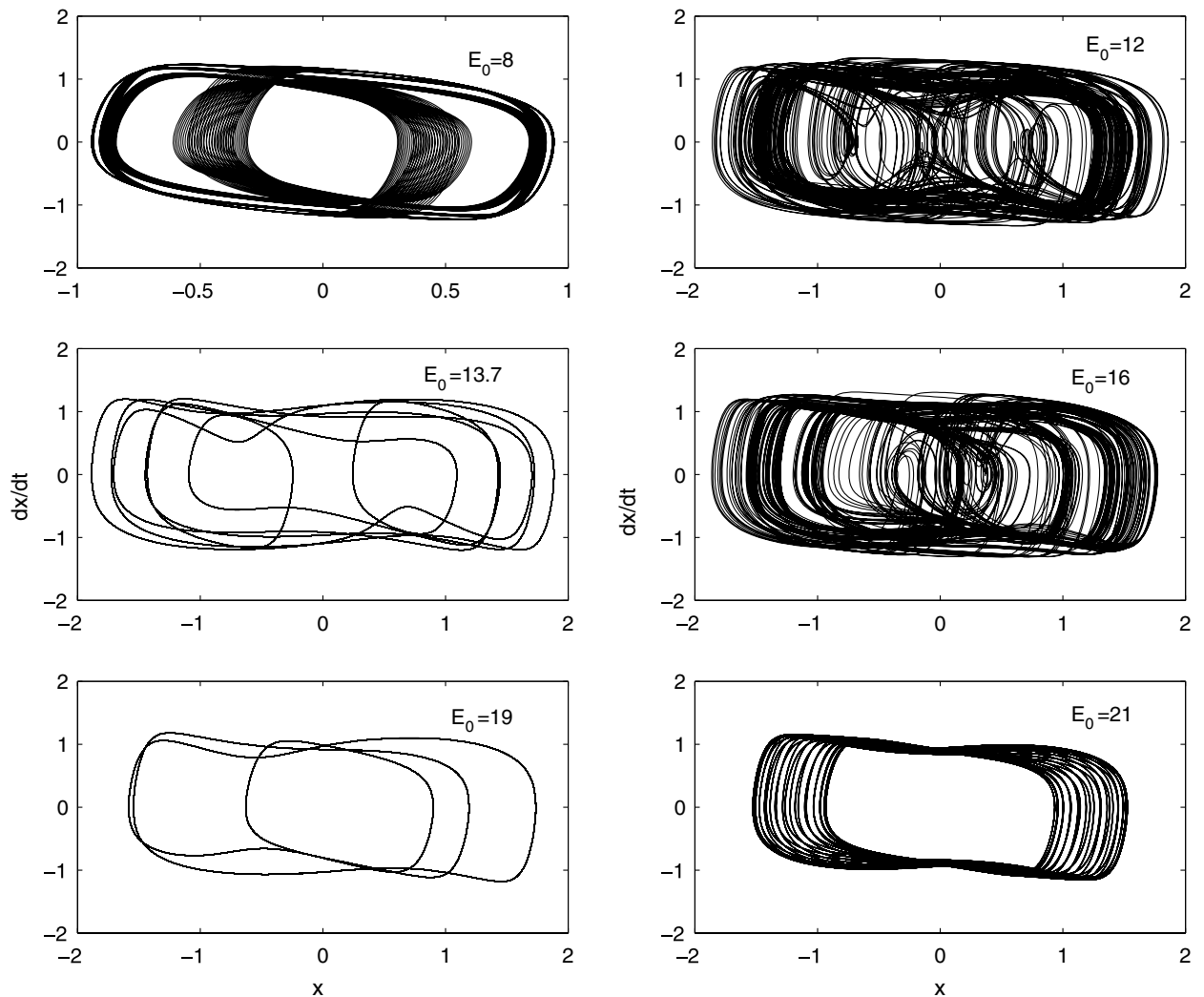


Fig. 11. Various phase portrait (v_x, x) for several different values of E_0 chosen in the stability chart, with the parameters of Fig. 6 and $\mu = 4$.

4.3. Bifurcation structures and stability chart

The aim of this subsection is to find some bifurcation structures and derive the stability chart in the forced self-sustained electromechanical model as the parameters of the system evolve. For this purpose, we numerically solve the equations of motion (15) and plot the resulting bifurcation diagrams as the amplitude of the external excitation E_0 varies. The stroboscopic time period used to map various transitions which appear in the model is $T = 2\pi/w$. With the following set of parameters $\mu = 2$; $\gamma_1 = 0.1$; $\lambda_1 = 0.4$; $\lambda_{11} = 0.2$; $w_1 = 1$; $\beta = 0.8$; $w = 1$; $n = 25$, our investigations show that the model exhibits chaotic behavior at $E_0 = 13.0$ and the chaotic phase portrait of the model is shown in Fig. 6. Fig. 7 shows a representative bifurcation diagram and the variation of the corresponding Lyapunov exponent as the amplitude E_0 varies. These curves are obtained by numerically solving Eq. (15) and the corresponding variational equations. The one dimensional Lyapunov exponent is defined by

$$Lya = \lim_{t \rightarrow \infty} \frac{\ln(d^{n+1}(t))}{t} \tag{22}$$

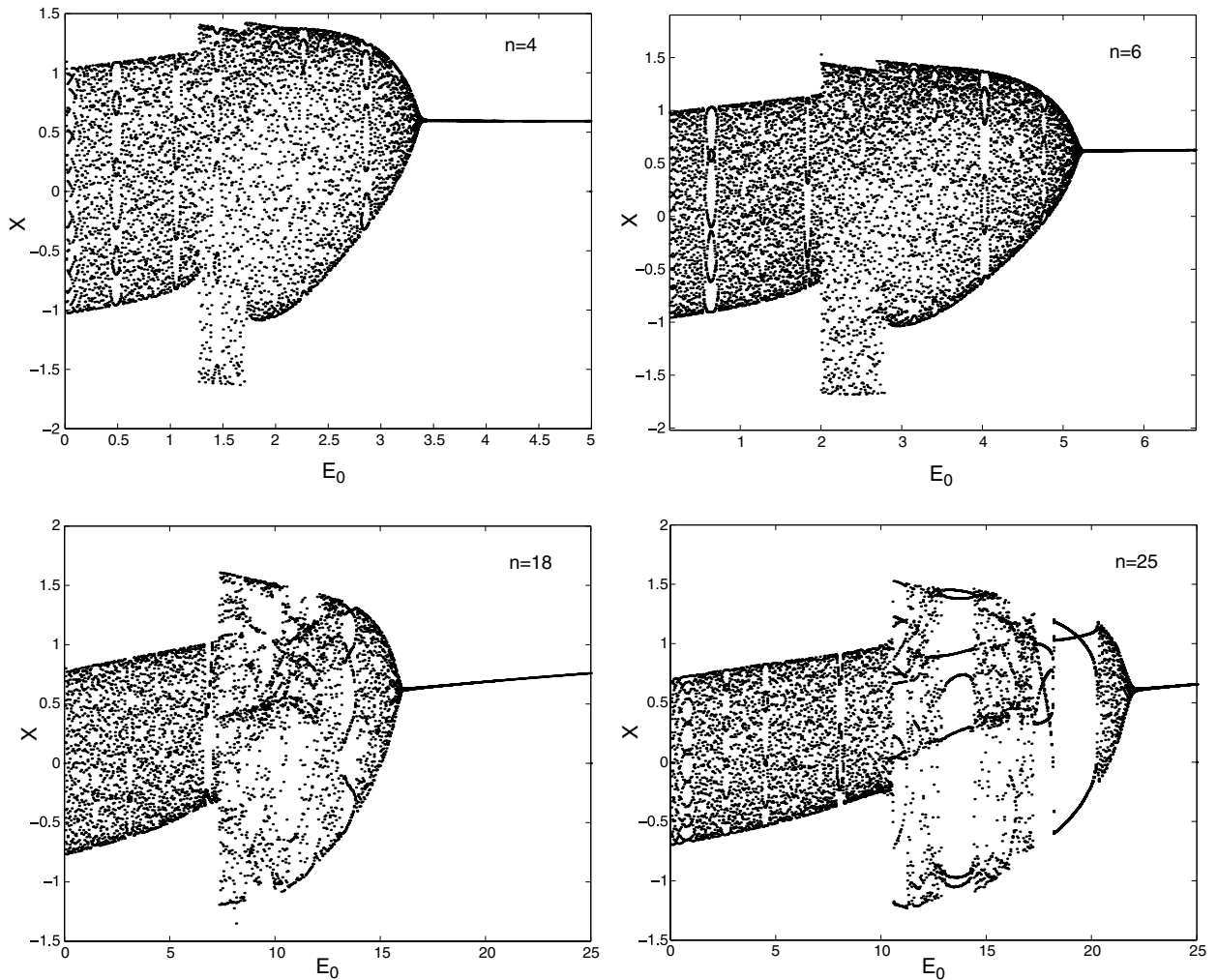


Fig. 12. Effects of the number n of the linear mechanical oscillators on the bifurcation structures of the model with the parameters of Fig. 6 and $\mu = 4$.

with

$$d^{n+1}(t) = \sqrt{dx^2 + d\dot{x}^2 + \sum_{i=1}^n dx_i^2 + \sum_{i=1}^n d\dot{x}_i^2}; \quad n = 25$$

where dx , $d\dot{x}$, dx_i and $d\dot{x}_i$ are respectively the variations of x , \dot{x} , x_i and \dot{x}_i . As the amplitude E_0 increases from zero, the amplitude of the quasi-periodic oscillations exists until $E_0 = 9.6$ where a period-3 orbit takes place. At $E_0 = 10.5$, the system bifurcates from a period-3 orbit to a chaotic orbit until $E_0 = 15.8$ where the period-7 orbit appears. From $E_0 = 18.0$, we have another region of chaotic motion. At $E_0 = 18.8$, the system passes from the chaotic orbit to the period-3 orbit and remains until $E_0 = 20.5$ where the quasi-periodic motion takes place before bifurcates to the period-1 orbit at $E_0 = 20.5$. The other bifurcation mechanisms which appear in the system are shown in Figs. 8 and 9 for respectively $\mu = 4$ and $\mu = 5$. In Fig. 10, we derive the stability chart using numerical simulations of the equations of motion (15) as well as the above transitions. The chart shown in the (μ, E_0) plane is traced out by using the bifurcation diagram when the amplitude E_0 varies for a fixed μ coefficient. One observes that as the amplitude E_0 increases, the forced self-sustained electromechanical system exhibits quasi-periodic, and period- m oscillations, and chaotic motions within a range of the μ coefficient (see Fig. 10). For example, for $\mu = 4$, we have the quasi-periodic oscillations for $E_0 \in [0.0; 10.6] \cup [12.3; 18.6]$, chaotic motions for $E_0 \in [10.6; 13] \cup [14.2; 17.2]$, period-7 orbit for $E_0 \in [14.2; 17.2]$, period-3 orbit for $E_0 \in [20.2; 22]$. Fig. 11 shows various phase portraits for several different values of E_0 chosen on the above mentioned domains, with the parameters of Fig. 6. The effects of the number of linear mechanical oscillators on the bifurcation structures are analyzed in Fig. 12 and it indicated that the bifurcation structures are affected with the increase of the number of linear mechanical oscillators. For example, with $n = 5; 6$, it appears that the forced self-sustained electromechanical system exhibit periodic and quasi-periodic oscillations, while for $n = 18; 25$, the system presents the chaotic behaviors together with the periodic and quasi-periodic oscillations. In summary, with the set of parameters used in this section, we find that the chaotic behaviors appears in the forced self-sustained electromechanical system only when n becomes large.

5. Conclusion

In this paper, we have studied the dynamics of the self-sustained electromechanical system with multiple functions, consisting of an electrical Rayleigh–Duffing oscillator magnetically coupled to linear mechanical oscillators. In the autonomous case, the amplitude of oscillatory states and their stability have been derived using the averaging method and it appears that the quenching of oscillations occurs for some sets of parameters. For the nonautonomous case, the harmonic balance method has enabled us to derive the amplitude of harmonic oscillations. The effects of the number of linear mechanical oscillators on the behaviors of the model have been analyzed. Our analytical results have been confirmed by numerical simulation. Various bifurcation structures showing different types of transitions from quasi-periodic motions to multi-periodic and chaotic motions have been drawn and the results have been presented in the stability chart.

Acknowledgements

Part of this work was done during the visit of R. Yamapi to the Abdus Salam International Centre for Theoretical Physics for a short visit (June 21–August 05, 2005) in the Condensed Matter and Statistical Physics research group. He would like to thank the Head of this research group for the invitation, hospitality and financial support. The authors would like to thank the anonym referee's for their interesting comments on the manuscript.

References

- [1] Parlitz U. Period-doubling cascades and devil's staircases of the driven Van der Pol oscillator. *Phys Rev A* 1987;36(3):1428–34.
- [2] Szemplińska-Stupnicka W, Rudowski Jersys. Neimark bifurcation, almost-periodicity and chaos in the forced Van der Pol–Duffing system in the neighbourhood of the principal resonance. *Phys Lett A* 1994;192:201–6.

- [3] Venkatesan A, Lukshmanan M. Bifurcation and chaos in the double-well Duffing–Van der Pol oscillator; numerical and analytical studies. *Phys Rev E* 1997;56(6):6321–30.
- [4] Camacho E, Rand R, Howland H. Dynamics of two Van der Pol oscillators coupled via bath. *Int J Solids Struct* 2004;41:2133–43.
- [5] Yamapi R, Chabi Orou JB, Wofo P. Harmonic oscillations, stability and chaos control in a non-linear electromechanical system. *J Sound Vib* 2003;259(5):1253–64.
- [6] Wofo P, Yamapi R, Chabi Orou JB. Dynamics of a nonlinear electromechanical system with multiple functions in series. *Commun Nonlinear Sci Numer Simul* 2005;10(3):229–51.
- [7] Yamapi R, Bowong S. Dynamics and chaos control in the self-sustained electromechanical device with and without discontinuity. *Commun Nonlinear Sci Numer Simul* 2006;11(3):355–75.
- [8] Nayfeh AH, Mook DT. *Nonlinear oscillations*. New York: Wiley-Interscience; 1979.
- [9] Hayashi C. *Nonlinear oscillations in physical systems*. New-York: Mc-Graw-Hill; 1964.
- [10] Oksasoglu A, Vavriv D. Interaction of low- and high-frequency oscillations in a nonlinear RLC circuit. *IEEE Trans Circ Syst-I* 1994;41:669–72.
- [11] Chedjou JC, Wofo P, Domngang S. Shilnikov chaos and dynamics of a self-sustained electromechanical transducer. *J Vib Acoust* 2001;123:170–4.
- [12] Hasler MJ. Electrical circuits with chaotic behavior. *Proc IEEE* 1987;75:1009–21.
- [13] Olson HF. *Acoustical engineering*. Princeton: Van Nostrand; 1967.
- [14] Korenev BG, Reznikav LM. *Dynamics vibration absorbers*. New york: Wiley; 1989.
- [15] Asfar KR. Quenching of self-excited vibrations. *Trans ASME J Vib Acoust Stress Reliab Des* 1989;121:130–3.